

# RoadFormer: Duplex Transformer for RGB-Normal Semantic Road Scene Parsing

Jiahang Li, Yikang Zhang, Peng Yun, Guangliang Zhou, Qijun Chen, Rui Fan<sup>✉</sup>

**Abstract**—The recent advancements in deep convolutional neural networks have shown significant promise in the domain of road scene parsing. Nevertheless, the existing works focus primarily on freespace detection, with little attention given to hazardous road defects that could compromise both driving safety and comfort. In this paper, we introduce RoadFormer, a novel Transformer-based data-fusion network developed for road scene parsing. RoadFormer utilizes a duplex encoder architecture to extract heterogeneous features from both RGB images and surface normal information. The encoded features are subsequently fed into a novel heterogeneous feature synergy block for effective feature fusion and recalibration. The pixel decoder then learns multi-scale long-range dependencies from the fused and recalibrated heterogeneous features, which are subsequently processed by a Transformer decoder to produce the final semantic prediction. Additionally, we release SYN-UDTIRI, the first large-scale road scene parsing dataset that contains over 10,407 RGB images, dense depth images, and the corresponding pixel-level annotations for both freespace and road defects of different shapes and sizes. Extensive experimental evaluations conducted on our SYN-UDTIRI dataset, as well as on three public datasets, including KITTI road, CityScapes, and ORFD, demonstrate that RoadFormer outperforms all other state-of-the-art networks for road scene parsing. Specifically, RoadFormer ranks first on the KITTI road benchmark. Our source code, created dataset, and demo video are publicly available at [mias.group/RoadFormer](https://mias.group/RoadFormer).

## I. INTRODUCTION

The advancements in machine intelligence have led to the extensive integration of autonomous driving technologies into various aspects of daily life and across multiple industries [1]. This integration spans a diverse range of products, including autonomous vehicles [2], mobile robots [3], and smart wheelchairs [4]. Recently, researchers in this field have shifted their focus towards enhancing both driving safety and comfort [5]. Road scene parsing, typically including pixel-level freespace and road defect detection, is of paramount importance in achieving these objectives [6].

Existing road scene parsing approaches predominantly fall under two categories: geometry-based and data-driven ones [1]. The algorithms in the former category typically leverage explicit geometric models to represent regions of interest (RoIs), and then proceed to optimize specific energy

This research was supported by the National Natural Science Foundation of China under Grant 62233013 (✉ *Corresponding author: Rui Fan*).

J. Li, Y. Zhang, G. Zhou, Q. Chen, and R. Fan are with the College of Electronics & Information Engineering, Shanghai Research Institute for Intelligent Autonomous Systems, Tongji University, Shanghai 201804, P. R. China (e-mails: {lijiahang617, yikangzhang, tj\_zgl, qjchen}@tongji.edu.cn, rui.fan@ieee.org).

P. Yun is with the Department of Computer Science & Engineering, the Hong Kong University of Science & Technology, Hong Kong SAR, P. R. China (e-mail: pyun@cse.ust.hk).

functions for accurate ROI extraction. For instance, the study presented in [7] employs a B-spline model to fit the road disparity map, which is subsequently projected onto a 2D v-disparity histogram for freespace detection. Additionally, the research presented in [8] introduces a disparity map transformation algorithm designed specifically for the effective detection of road defects.

With the proliferation of deep learning techniques, convolutional neural networks (CNNs) have emerged as a potent tool for road scene parsing, often treating it as a binary or ternary semantic segmentation task [1], [9]. These methods have demonstrated significant performance gains over traditional geometry-based approaches. For example, the study detailed in [10] employs an encoder-decoder CNN architecture to realize freespace detection by segmenting RGB images in the bird's eye view. Nonetheless, the results achieved by this approach fall short of satisfactory performance benchmarks. To address this limitation, ensuing research has explored the utilization of data-fusion networks with duplex encoder architectures as a feasible strategy to improve the road scene parsing accuracy. Specifically, [11] extracts heterogeneous features from RGB-Depth data, and subsequently performs feature fusion through a basic element-wise summation operation. The fusion of disparate feature types brings a more comprehensive understanding of the given scenario, resulting in superior performance over earlier single-modal networks. Similar to [11], SNE-RoadSeg series [1], [12] perform RGB-Normal feature fusion through element-wise summation. By employing a duplex ResNet [13] in conjunction with a strong densely-connected decoder, the SNE-RoadSeg series achieve state-of-the-art (SoTA) performance on the KITTI road benchmark [14].

Within the domain of computer vision, Transformers have empirically demonstrated their potential to outperform CNNs, particularly when large-scale datasets are available for training [15]–[17]. This advantage can be attributed to the self-attention mechanisms inherent to Transformers, which provide a notably more efficient strategy for global context modeling compared to conventional CNNs [18]. OFF-Net [19] is the first attempt to apply the Transformer architecture for road scene parsing. With abundant off-road training data, it outperforms CNN-based algorithms. Unfortunately, OFF-Net utilizes a lightweight CNN-based decoder instead of a Transformer-based one. We believe that the adoption of a Transformer-based decoder has the potential to elevate the upper limit of road scene parsing performance. We also observe its unsatisfactory performance on urban road scenes, especially when the data are limited.

Therefore, in this paper, we introduce RoadFormer, a novel duplex Transformer architecture designed for data-fusion semantic road scene parsing. Benefiting from its duplex encoder, RoadFormer can extract abstract and informative heterogeneous features from RGB-Normal data. Additionally, we introduce a novel Heterogeneous Feature Synergy Block (HFSB), which draws upon the self-attention mechanism to improve feature fusion and recalibration. Extensive experiments conducted on public freespace detection datasets demonstrate that RoadFormer achieves improved overall performance than existing SoTA networks. Specifically, RoadFormer ranks first on the KITTI road benchmark [14]. In contrast to existing studies and their utilized datasets in the domain of road scene parsing [2], [20], [21], which predominantly characterize freespace as undamaged, the aspect of road defects remains notably under-explored. This oversight can be attributed, in part, to the sporadic nature of road defects, making the collection of comprehensive, large-scale datasets containing both RGB and depth images challenging. To this end, we create SYN-UDTIRI, a large-scale, multi-source synthetic dataset, specifically for the understanding of road scenes inclusive of defects. By publishing this dataset, we not only advance the scope of semantic parsing in road scenes but also open up new avenues for data-driven research, thereby demonstrating the capabilities of our proposed RoadFormer.

## II. RELATED WORK

### A. Single-Modal Networks

Fully convolutional network (FCN) [22] pioneered the utilization of CNNs for single-modal semantic segmentation. Although FCN significantly outperforms traditional methods based on hand-crafted features, its performance is constrained by the absence of multi-scale feature utilization [23]. To address this limitation, Deeplabv3+ [24] employs atrous convolution with different dilation rates, thereby enhancing the network's capability to encode contextual features across multiple scales. The high-resolution network (HRNet) [25] employs an alternative strategy for multi-scale feature encoding. Instead of using the detrimental resizing of feature maps, HRNet integrates low-resolution branches in parallel with the high-resolution main branch to achieve multi-scale feature extraction.

Transformers have been applied to semantic segmentation tasks due to their superior global aggregation capabilities over CNNs [26]. Segmentation Transformer (SETR) [27] is the first Transformer-based semantic segmentation network. Building on the success of Vision Transformer (ViT) [28], it tokenizes images into patches and feeds them into Transformer blocks. These encoded features are then gradually restored through upsampling convolution to achieve pixel-level classification. SegFormer [17] introduces a multi-scale Transformer encoder for semantic segmentation, which stacks Transformer blocks and inserts convolutional layers between them. Compared to SETR, SegFormer improves segmentation performance when dealing with objects of varying sizes. Additionally, MaskFormer [29] introduces a new paradigm

for semantic segmentation. Rather than adhering to standard per-pixel classification methods, this architecture addresses semantic segmentation tasks by segmenting an image into a set of masks. In detail, MaskFormer employs a multi-scale Transformer decoder that outputs the mask for each class using refined queries in parallel, outperforming previous per-pixel classification approaches. This query-based prediction fashion is also adopted in our proposed method and has demonstrated improved performance over SoTA CNNs in terms of segmentation accuracy.

### B. Data-Fusion Networks

Data-fusion networks effectively leverage heterogeneous features extracted from RGB images and spatial geometric information to improve segmentation performance. FuseNet [11] was the first attempt to incorporate depth information into semantic segmentation, using separate CNN encoders for RGB and depth images and fusing their features through element-wise summation. MFNet [30] strikes a balance between speed and accuracy in driving scene parsing through RGB-Thermal fusion. Similarly, RTFNet [31] also uses RGB-Thermal data as inputs and designs a robust decoder that utilizes shortcuts to produce clear boundaries while retaining detailed features. Inspired by [11], SNE-RoadSeg [1] and SNE-RoadSeg+ [12] incorporate surface normal information into freespace detection. This series employs densely connected skip connections to enhance feature extraction in their decoder, thereby achieving SoTA performance compared to other approaches. Drawing on the success of single-modal Transformer models, OFF-Net [19] was the first attempt to apply Transformer architecture for data-fusion freespace detection. It utilizes a SegFormer [17] encoder to generate RGB and surface normal features, thereby outperforming SoTA CNNs in off-road freespace detection. Expanding upon these foundational prior arts, our RoadFormer also adopts the data-fusion paradigm but differentiates itself by employing a novel Transformer architecture for semantic road scene parsing. Additionally, RoadFormer utilizes a novel feature synergy block, leading to superior performance over all other data-fusion networks on four road scene parsing datasets.

## III. METHODOLOGY

This section details RoadFormer, a robust and powerful data-fusion Transformer architecture for road scene parsing. As depicted in Fig. 1, RoadFormer consists of (1) a duplex encoder to learn heterogeneous features from RGB-Normal data, (2) a feature synergy block to fuse and recalibrate the encoded heterogeneous features, (3) a pixel decoder to learn long-range dependencies from recalibrated features, and (4) a Transformer decoder to achieve final semantic prediction by refining query features using outputs of the pixel decoder.

### A. Duplex Encoder

In line with our previous works [1], [4], [12], we employ a duplex-encoder structure to extract multi-scale heterogeneous features. One encoder focuses on learning color and texture

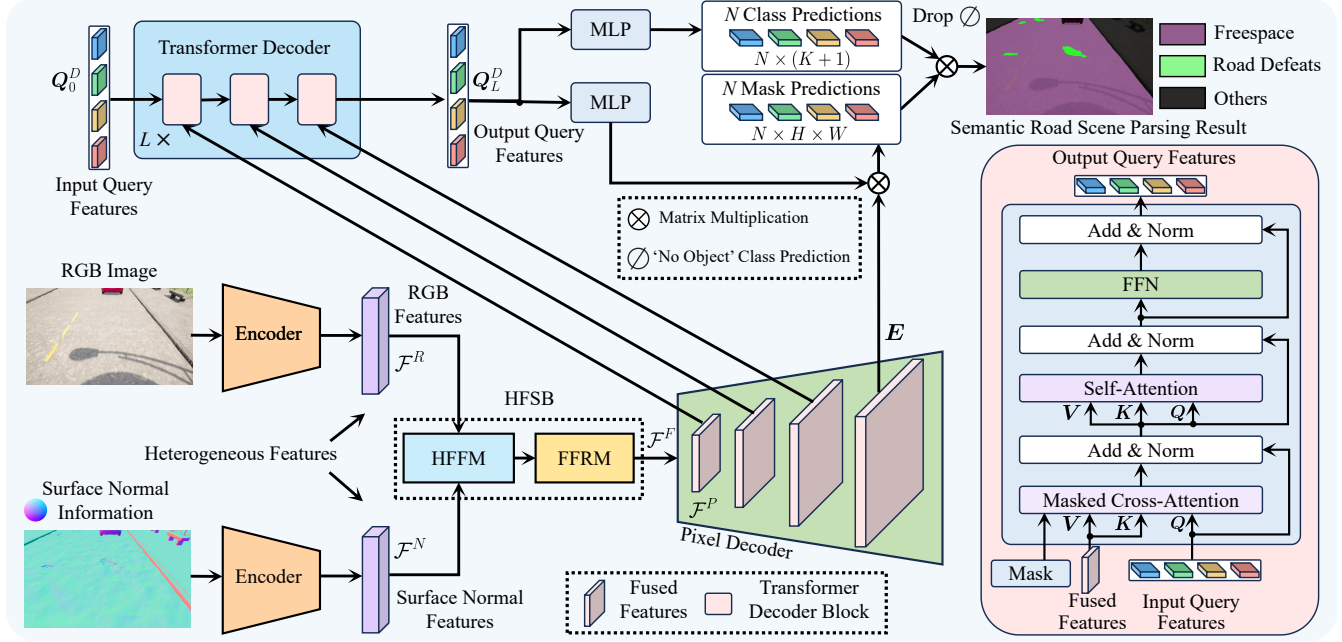


Fig. 1: An overview of our proposed RoadFormer architecture.

features  $\mathcal{F}^R = \{\mathbf{F}_1^R, \dots, \mathbf{F}_k^R\}$  from RGB images  $\mathbf{I}^R \in \mathbb{R}^{H \times W \times 3}$ , while the other encoder specializes in acquiring representations  $\mathcal{F}^N = \{\mathbf{F}_1^N, \dots, \mathbf{F}_k^N\}$  of planar characteristics from the surface normal information  $\mathbf{I}^N \in \mathbb{R}^{H \times W \times 3}$ , where  $H$  and  $W$  represent the height and width of the input image, respectively.  $\mathbf{F}_i^{R,N} \in \mathbb{R}^{\frac{H}{S_i} \times \frac{W}{S_i} \times C_i}$  represents the  $i$ -th feature maps, and  $C_i$  and  $S_i = 2^{i+1}$  ( $i \in [1, k] \cap \mathbb{Z}$ ) denote the corresponding channel and stride numbers, respectively. Our duplex encoder is compatible with both Transformer-based and CNN-based backbones. For this study, we utilize Swin Transformer [16] and ConvNeXt [32] as our backbones, respectively. The performance comparison of these backbones is presented in Sect. I.

## B. Heterogeneous Feature Synergy Block

1) *Heterogeneous Feature Fusion Module (HFFM)*: Conventional duplex networks typically fuse heterogeneous features using basic element-wise addition or feature concatenation operations [4]. Nevertheless, we contend that such a simplistic feature fusion strategy might not fully exploit the inherent potential of heterogeneous features. The recent surge in the popularity of Transformer architectures for multi-modal visual-linguistic tasks [33], [34] can be attributed to their powerful attention mechanisms that enable effective joint representations across modalities [35]. Drawing inspiration from these prior arts, our objective is to utilize attention mechanisms to enhance the fusion of heterogeneous features extracted by the duplex encoder mentioned above. To this end, we introduce HFFM (see Fig. 2 (a)), which builds upon the self-attention mechanisms of Transformers to achieve effective fusion of  $\mathcal{F}^R$  and  $\mathcal{F}^N$  through token interactions. Our HFFM can be formulated as follows:

$$\mathbf{F}_i^H = \text{Reshape} \left( \text{Norm} \left( \text{Softmax} \left( \mathbf{Q}_i^C \mathbf{K}_i^{C^\top} \right) \kappa_i \mathbf{V}_i^C + \mathbf{F}_i^C \right) \right), \quad (1)$$

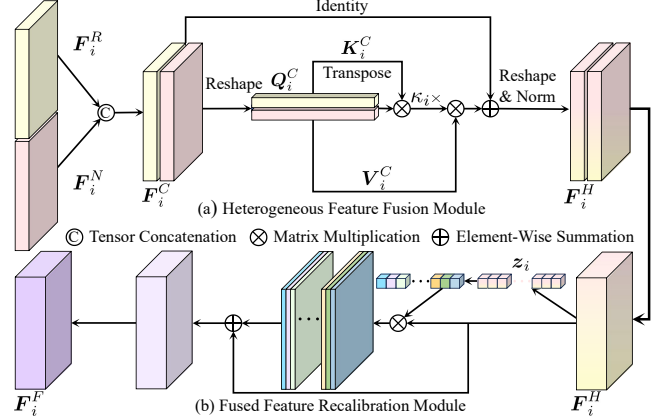


Fig. 2: Heterogeneous feature synergy block.

where  $\mathbf{F}_i^R$  and  $\mathbf{F}_i^N$  are concatenated and reshaped to form  $\mathbf{F}_i^C \in \mathbb{R}^{2C_i \times \frac{H}{S_i} \frac{W}{S_i}}$ , which is then identically mapped to query  $\mathbf{Q}_i^C$ , key  $\mathbf{K}_i^C$ , and value  $\mathbf{V}_i^C$  embeddings, and  $\mathbf{F}_i^H \in \mathbb{R}^{\frac{H}{S_i} \times \frac{W}{S_i} \times 2C_i}$  denotes the output of the HFFM. Additionally, following [36], we introduce a learnable coefficient  $\kappa_i$  to adaptively adjust the attention significance, enabling a more flexible fusion of heterogeneous features.

2) *Fused Feature Recalibration Module (FFRM)*: In conventional single-encoder architecture designs, multi-channel features do not all contribute positively to semantic predictions. In fact, some noisy or irrelevant feature maps may even degrade the model's performance. In this regard, the squeeze-and-excitation block (SEB) [37] was designed to model the inter-dependencies between the channels of convolutional features via a channel attention mechanism. This allows the network to focus on more informative features while downplaying the less important ones. A similar issue also occurs in our work: the heterogeneous features extracted by our duplex encoder may focus on different components in

the scene, and the fusion of these features might potentially undermine the saliency of the original key features or even produce irrelevant features [38]. To this end, we develop FFRM (see Fig. 2 (b)) based on SEB to recalibrate the fused heterogeneous features. In particular, we add a residual connection atop the SEB to enhance its training [13] and introduce an additional point-wise convolution to realize the flexible computation of correlations between the recalibrated features [39]. Our FFRM can be formulated as follows:

$$\mathbf{F}_i^F = \text{Conv}_{1 \times 1} \left( \mathbf{F}_i^H + \left( \mathbf{O} \text{ Sigmoid} \left( \text{Conv}_{1 \times 1}(\mathbf{z}_i) \right) \right) \odot \mathbf{F}_i^H \right), \quad (2)$$

where  $\mathbf{O} \in \mathbb{R}^{\frac{H}{S_i} \times \frac{W}{S_i} \times 1 \times 1}$  represents a matrix of ones,  $\odot$  denotes the Hadamard product operation,  $\mathbf{z}_i = [z_{i,1}, \dots, z_{i,2C_i}] \in \mathbb{R}^{1 \times 1 \times 2C_i}$  stores the average pooling results of each feature map in  $\mathbf{F}_i^H$ , and

$$z_{i,j} = \frac{S_i^2}{HW} \sum_{h=1}^{\frac{H}{S_i}} \sum_{w=1}^{\frac{W}{S_i}} \mathbf{F}_i^H(h, w, j). \quad (3)$$

The performance comparison between our proposed HFFM, FFRM, and SE block is discussed in Sect. II.

### C. Pixel Decoder

Following [40], we incorporate a pixel decoder to improve multi-scale feature modeling for  $\mathcal{F}^F = \{\mathbf{F}_1^F, \dots, \mathbf{F}_k^F\}$  to generate  $\mathcal{F}^P = \{\mathbf{F}_1^P, \dots, \mathbf{F}_n^P\}$  ( $n < k$ ), where  $\mathbf{F}_i^P \in \mathbb{R}^{\frac{H}{S_i} \times \frac{W}{S_i} \times C}$ . It also serves the function of upsampling low-resolution features in  $\mathcal{F}^F$  to generate a high-resolution per-pixel embedding  $\mathbf{E}$ , which is then used by the Transformer decoder to guide the mask prediction. Given the recent success of multi-scale deformable attention Transformer [41], [42], we adopt a similar architecture for our pixel decoder.

### D. Transformer Decoder

We utilize a Transformer-based decoder to recursively update the input query feature  $\mathbf{Q}_l^D$  based on the multi-scale feature maps  $\mathbf{F}_2^P$  to  $\mathbf{F}_n^P$  extracted by the pixel decoder. The per-pixel embedding  $\mathbf{E}$  is used to guide mask predictions. One Transformer decoder layer consists of a sequence of operations: (1) the query feature  $\mathbf{Q}_l^D = f_Q(\mathbf{X}_{l-1}) \in \mathbb{R}^{N \times C}$  is obtained through a linear transformation operation  $f_Q(\cdot)$ , where  $\mathbf{X}_0 \in \mathbb{R}^{N \times C}$  is the initial query feature; (2) the key feature  $\mathbf{K}_l^D = f_K(\mathbf{F}_l^P) \in \mathbb{R}^{\frac{H}{S_i} \frac{W}{S_i} \times C}$  and value feature  $\mathbf{V}_l^D = f_V(\mathbf{F}_l^P) \in \mathbb{R}^{\frac{H}{S_i} \frac{W}{S_i} \times C}$  are obtained through two linear transformation operations  $f_K(\cdot)$  and  $f_V(\cdot)$ , respectively; (3)  $\mathbf{Q}_l^D$ ,  $\mathbf{K}_l^D$ , and  $\mathbf{V}_l^D$  are subsequently processed by a masked cross-attention mechanism, expressed as follows:

$$\mathbf{X}_l = \text{Softmax}(\mathbf{M}_{l-1} + \mathbf{Q}_l^D \mathbf{K}_l^{D \top}) \mathbf{V}_l^D + \mathbf{X}_{l-1}, \quad (4)$$

where  $\mathbf{M}_{l-1} \in \mathbb{R}^{N \times \frac{H}{S_i} \frac{W}{S_i}}$  (containing only the values of 0 or  $-\infty$ ) denotes the output of the resized mask prediction obtained from the  $(l-1)$ -th Transformer decoder layer (readers can refer to [40] for more details); (4) the masked cross-attention results are subsequently processed by a self-attention mechanism, and ultimately passed through a

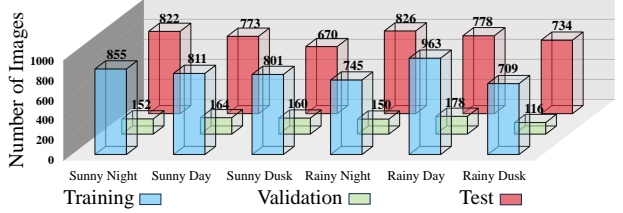


Fig. 3: Data distribution in the SYN-UDTIRI dataset.

feedforward network (FFN). Multi-scale feature maps  $\mathbf{F}_2^P$  to  $\mathbf{F}_n^P$  are fed to their corresponding decoder layer, and the entire process is iterated  $L$  times to yield the final updated query features. Following [43], the final query feature  $\mathbf{Q}_L^D$  produced by the Transformer decoder is mapped into a space of dimension  $(K+1)$  for class predictions by a multi-layer perceptron (MLP), where  $K$  represents the total number of classes to be predicted, plus an additional class representing “no object”. The mask prediction is then obtained by performing a dot product operation between the mask embedding  $\text{MLP}(\mathbf{Q}_L^D)$  (also generated by MLP) and the per-pixel embedding  $\mathbf{E}$ . Finally, the semantic road scene parsing result is obtained by performing a simple matrix multiplication operation (followed by an argmax function) between the mask and class predictions.

### E. Loss Function

We follow [40] to train our proposed RoadFormer by minimizing the following loss function:

$$\mathcal{L} = \lambda_{\text{mask}} (\lambda_{\text{ce}} \mathcal{L}_{\text{ce}} + \lambda_{\text{dice}} \mathcal{L}_{\text{dice}}) + \lambda_{\text{cls}} \mathcal{L}_{\text{cls}}, \quad (5)$$

where  $\mathcal{L}_{\text{ce}}$  and  $\mathcal{L}_{\text{dice}}$  are the binary cross-entropy loss and the dice loss, respectively.  $\mathcal{L}_{\text{cls}}$  is the classification loss, and the weighting factors  $\lambda_{\text{mask}}$ ,  $\lambda_{\text{ce}}$ ,  $\lambda_{\text{dice}}$ , and  $\lambda_{\text{cls}}$  serve to balance the respective contributions of the different loss components to the overall loss. These are set in accordance with [40].

## IV. EXPERIMENTS

### A. Datasets

1) **SYN-UDTIRI**: Owing to the lack of well-annotated, large-scale datasets, created specifically for road scene parsing (freespace and road defect detection), we create a synthetic dataset, referred to as SYN-UDTIRI, using the CARLA simulator [44]. The principal contribution of this dataset lies in the integration of digital twins of road potholes acquired from the real world using our previously published 3D geometry reconstruction algorithm [45], [46]. Moreover, to better simulate the roughness of actual roads, we introduce random Perlin noise [47] to the road data. We generate six driving scenarios, including sunny day, dusk, and night, as well as rainy day, dusk, and night, with respect to different illumination and weather conditions. Additionally, we deploy a simulated stereo rig (baseline: 0.5m) onto a moving vehicle to acquire over 10K pairs of stereo road images (resolution:  $720 \times 1,280$  pixels), along with their corresponding depth images, surface normal information, and semantic annotations, including three categories: freespace, road defect, and other objects. More details on the SYN-UDTIRI dataset are given in Fig. 3.

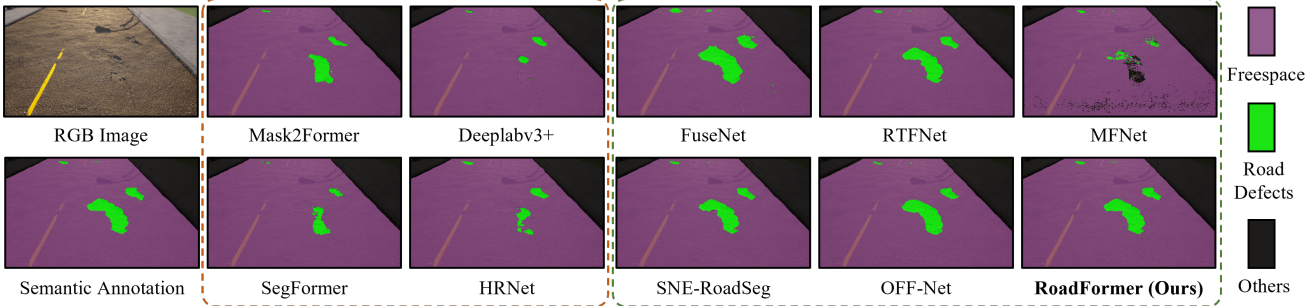


Fig. 4: Qualitative comparison between our proposed RoadFormer and other SoTA networks on the SYN-UDTIRI dataset.

TABLE I: Ablation study on backbone selection.

Dataset	Backbone	IoU (%)	Fsc (%)	Pre (%)	Rec (%)
SYN-UDTIRI	ConvNeXt	<b>93.38</b>	<b>96.58</b>	96.58	<b>96.74</b>
	Swin	93.18	96.47	<b>96.59</b>	96.35
CityScapes	ConvNeXt	<b>95.80</b>	<b>97.86</b>	<b>97.74</b>	<b>97.97</b>
	Swin	94.69	97.27	97.25	97.29

TABLE II: Ablation study demonstrating the effectiveness of our proposed HFFM and FFRM.

SEB	HFFM	FFRM	IoU (%)	Acc (%)	Fsc (%)	Pre (%)	Rec (%)
✗	✗	✗	95.11	96.87	97.50	98.12	96.87
✓	✗	✗	95.45	97.40	97.67	<b>97.95</b>	97.40
✗	✗	✓	95.49	97.59	97.69	97.79	97.59
✗	✓	✗	95.34	97.67	97.61	97.55	97.67
✗	✓	✓	<b>95.80</b>	<b>97.97</b>	<b>97.86</b>	97.74	<b>97.97</b>

2) **KITTI Road**: The KITTI road [14] dataset contains 289 pairs of stereo images and their corresponding LiDAR point clouds for model training and validation. It also provides a comparable amount of testing data without semantic annotations. We follow a similar data pre-processing strategy as detailed in [1]. We fine-tune our proposed RoadFormer for the test set result submission to the KITTI road benchmark.

3) **CityScapes**: The CityScapes [21] dataset is a widely utilized urban scene dataset, containing 2,975 stereo training images and 500 validation images, with well-annotated semantic annotations. Due to the limited sample size of the KITTI road dataset, we conducted additional experiments on the CityScapes dataset to further demonstrate the effectiveness of our proposed RoadFormer on large-scale datasets. All the experimental results are obtained using the validation set. It is noteworthy that the corresponding surface normal information is derived from depth images obtained using RAFT-Stereo [48] trained on the KITTI [49] dataset.

4) **ORFD**: The ORFD [19] dataset is designed specifically for off-road freespace detection. It contains 12,198 RGB images and their corresponding LiDAR point clouds, collected across various scenes, under different weather and illumination conditions. We follow the data splitting and pre-processing strategies (except for surface normal estimation) detailed in [19] for our experiments.

#### B. Experimental Setup and Evaluation Metrics

In our experiments, we compare our proposed RoadFormer with four single-modal networks and five data-fusion networks. The single-modal networks are trained using RGB images, while the data-fusion networks are trained using

TABLE III: Quantitative results on the SYN-UDTIRI dataset.

	Subset	Method	IoU (%)	Fsc (%)	Pre (%)	Rec (%)
RGB	Validation	Mask2Former	64.29	78.27	83.0	74.05
		SegFormer	52.46	68.82	70.13	67.55
		Deeplabv3+	52.94	69.23	75.23	64.12
		HRNet	52.92	69.21	79.46	61.30
	Test	Mask2Former	46.91	63.87	73.59	56.41
		SegFormer	36.34	53.31	57.23	49.89
		Deeplabv3+	34.76	51.58	62.54	43.90
		HRNet	35.47	52.37	69.09	42.16
RGB-Normal	Validation	FuseNet	67.30	80.40	68.30	<b>97.80</b>
		SNE-RoadSeg	92.00	95.80	96.30	95.40
		RTFNet	90.30	94.90	94.10	95.70
		OFF-Net	83.90	91.30	91.70	90.80
		MFNet	89.50	94.50	95.70	93.30
		<b>RoadFormer</b>	<b>93.35</b>	<b>96.56</b>	<b>96.53</b>	96.59
	Test	FuseNet	70.70	82.90	72.10	<b>97.50</b>
		SNE-RoadSeg	92.10	95.90	<b>96.70</b>	95.10
		RTFNet	90.50	95.00	95.50	94.50
		OFF-Net	83.80	91.20	91.90	90.50
		MFNet	87.70	93.50	96.20	90.90
		<b>RoadFormer</b>	<b>93.51</b>	<b>96.65</b>	96.61	96.69

TABLE IV: Quantitative results on the CityScapes dataset.

	Method	IoU (%)	Fsc (%)	Pre (%)	Rec (%)	mIoU (%)
RGB	Mask2Former	93.84	96.82	97.14	96.51	74.80
	SegFormer	93.98	96.90	96.02	97.79	64.51
	Deeplabv3+	93.82	96.81	96.99	96.63	68.66
	HRNet	94.06	96.94	96.29	97.59	70.10
RGB-Normal	FuseNet	91.60	95.60	96.00	95.30	52.70
	SNE-RoadSeg	93.80	96.80	96.10	97.50	53.40
	RTFNet	94.10	96.90	96.30	97.60	49.60
	OFF-Net	89.60	94.50	93.40	95.70	39.20
	MFNet	92.10	95.90	94.10	97.70	49.30
	<b>RoadFormer</b>	<b>95.80</b>	<b>97.86</b>	<b>97.74</b>	<b>97.97</b>	<b>76.20</b>

both RGB images and surface normal information (estimated using D2NT [50] owing to its superior accuracy compared to other methods). All the networks undergo training for the same number of epochs. For RoadFormer training, we utilize the AdamW optimizer [51] with a polynomial learning rate decay strategy [52]. The learning rate begins at  $10^{-4}$  with a weight decay of  $5 \times 10^{-2}$ . We apply learning rate multipliers of  $10^{-1}$  to both ConvNeXt [32] and Swin [16] backbones.

We utilize five common metrics to quantitatively evaluate the performance of our models: accuracy (Acc), precision (Pre), recall (Rec), intersection over union (IoU), and F-score (Fsc). We refer readers to our previous work [1] for more details on these metrics. Additionally, the evaluation metrics used for the KITTI road benchmark can be found on its official webpage: [cvlibs.net/datasets/kitti/eval\\_road.php](http://cvlibs.net/datasets/kitti/eval_road.php).

### C. Ablation Study

Although recent studies, such as [40] and [42], often combine the widely used Swin Transformer encoder with a Transformer decoder, we hypothesize that the Swin Transformer might not be the optimal choice for all tasks. Therefore, we perform an ablation study on SYN-UDTIRI and CityScapes to compare the performance of ConvNeXt and Swin Transformer for encoder backbone selection. As shown in Table I, ConvNeXt demonstrates superior performance over Swin, achieving improvements of 0.20%-1.11% in terms of IoU and 0.11%-0.80% in terms of F-score. These results suggest that our proposed RoadFormer is compatible with both CNN-based and Transformer-based backbones, and ConvNeXt is generally a preferable option for road scene parsing. Therefore, in the following experiments, we utilize ConvNeXt as our backbone network.

Given that the design of FFRM is inspired by SEB, we first compare the performance of our RoadFormer when incorporated with either SEB or FFRM. Furthermore, we also evaluate the individual effectiveness of HFFM and FFRM, as well as their compatibility. The results shown in Table II indicate that (1) FFRM outperforms SEB, achieving an improvement of 0.04% in terms of IoU, (2) HFFM yields a 0.23% higher IoU compared to the baseline setup, and (3) the combined utilization of HFFM and FFRM modules results in better performance than using these modules independently.

### D. Experimental Results

The quantitative results on the SYN-UDTIRI, CityScapes, ORFD, and KITTI Road datasets are presented in Tables III, IV, V, and VI, respectively. Additionally, we also present readers with the qualitative results on the SYN-UDTIRI dataset in Fig. 4. These results suggest that our proposed RoadFormer outperforms all other SoTA networks across all four datasets, demonstrating its exceptional performance and robustness in effectively parsing various types of road scenes, including synthetic roads with defects, urban roads, and rural roads. As shown in Table III, it is evident that data-fusion networks demonstrate considerably improved robustness compared to single-modal networks, particularly in road defect detection. We exclude the freespace detection results for comparison due to the closely matched performance across all networks in this task (the single-modal and data-fusion networks achieve IoUs of over 98.5% and 99.5%, respectively). As expected, data-fusion networks achieve better generalization ability compared to single-modal networks. This improvement is attributed to geometric features extracted from surface normal information. Despite achieving SoTA accuracy, RoadFormer yields an inference speed of  $\sim 20$  FPS when processing images at a resolution of  $352 \times 640$  pixels on an NVIDIA RTX 3090 GPU.

Additionally, the results on the CityScapes dataset somewhat exceed our expectations. The performance of the single-modal networks, with the IoU fluctuating within a range of 0.2%, is quite comparable to that of the data-fusion networks. To our surprise, all single-modal networks outperform data-fusion networks, except for RTFNet and our

TABLE V: Quantitative results on the ORFD dataset.

	Method	IoU (%)	Fsc (%)	Pre (%)	Rec (%)
RGB-Normal	FuseNet	59.00	74.20	59.30	<b>99.10</b>
	SNE-RoadSeg	79.50	88.60	90.30	86.90
	RTFNet	90.70	95.10	93.80	96.50
	OFF-Net	81.80	90.00	84.20	96.70
	MFNet	81.70	89.90	89.60	90.30
	<b>RoadFormer</b>	<b>92.51</b>	<b>96.11</b>	<b>95.08</b>	97.17

TABLE VI: Comparison of SoTA algorithms published on the KITTI road benchmark.

Method	MaxF (%)	AP (%)	Pre (%)	Rec (%)	Rank
NIM-RTFNet [53]	96.02	94.01	96.43	95.62	13
HID-LS [54]	93.11	87.33	92.52	93.71	33
LC-CRF [55]	95.68	88.34	93.62	97.83	15
SNE-RoadSeg [1]	96.75	94.07	96.90	96.61	8
SNE-RoadSeg+ [12]	97.50	93.98	<b>97.41</b>	97.58	2
PLB-RD [56]	97.42	<b>94.09</b>	97.30	97.54	3
LRDNet+ [57]	96.95	92.22	96.88	97.02	4
DFM-RTFNet [4]	96.78	94.05	96.62	96.93	7
<b>RoadFormer</b>	<b>97.50</b>	93.85	97.16	<b>97.84</b>	<b>1</b>

RoadFormer. We speculate that these unexpected results could be attributed to inaccuracies in the disparity maps used for surface normal estimation, as they are directly obtained from pretrained stereo matching networks. The previous data-fusion networks employ basic element-wise addition or feature concatenation operations for feature fusion, leading to performance degradation when surface normal information is inaccurate. In contrast, benefiting from the adaptive fusion and recalibration of heterogeneous features via our designed HFSB, our RoadFormer achieves the highest scores across all metrics, including the mean IoU (mIoU) computed across 19 categories in the full-pixel semantic segmentation task.

Moreover, we observe that the performances of data-fusion networks differ significantly on the ORFD dataset. This is likely due to the challenge of labeling accurate off-road semantic ground truth. The inaccurate annotations may introduce ambiguities during the model training process. Finally, we submit the test set results produced by RoadFormer to the KITTI road benchmark for performance comparison. As shown in Table VI, RoadFormer demonstrates superior performance compared to all previously published methods.

## V. CONCLUSION

This paper presents RoadFormer, a powerful data-fusion Transformer architecture designed for road scene parsing. It contains a duplex encoder, a novel feature synergy block, and Transformer-based decoders. Compared to previous works, RoadFormer demonstrates the effective fusion of heterogeneous features and improved accuracy. It outperforms all existing semantic segmentation networks on our newly created SYN-UDTIRI dataset and three public datasets, while ranking first on the KITTI road benchmark. As critical components of RoadFormer, feature fusion using self-attention has proven superior to CNNs for road scene parsing, and we aim to investigate its potential for more common scene parsing tasks in the future. On the other hand, although achieving high accuracy, the real-time performance of data-fusion networks still needs improvement, which we will leave to future work.

## REFERENCES

[1] R. Fan *et al.*, “SNE-RoadSeg: Incorporating Surface Normal Information into Semantic Segmentation for Accurate Freespace Detection,” in *European Conference on Computer Vision (ECCV)*. Springer, 2020, pp. 340–356.

[2] A. Geiger *et al.*, “Vision meets robotics: The KITTI dataset,” *The International Journal of Robotics Research*, vol. 32, no. 11, pp. 1231–1237, 2013.

[3] J. Li *et al.*, “Towards Broad Learning Networks on Unmanned Mobile Robot for Semantic Segmentation,” in *2022 International Conference on Robotics and Automation (ICRA)*. IEEE, 2022, pp. 9228–9234.

[4] H. Wang *et al.*, “Dynamic Fusion Module Evolves Drivable Area and Road Anomaly Detection: A Benchmark and Algorithms,” *IEEE Transactions on Cybernetics*, vol. 52, no. 10, pp. 10750–10760, 2021.

[5] Y. Du *et al.*, “Velocity Control Strategies to Improve Automated Vehicle Driving Comfort,” *IEEE Intelligent Transportation Systems Magazine*, vol. 10, no. 1, pp. 8–18, 2018.

[6] B. Barabino *et al.*, “Standing Passenger Comfort: A New Scale for Evaluating the Real-Time Driving Style of Bus Transit Services,” *IEEE Transactions on Intelligent Transportation Systems*, vol. 20, no. 12, pp. 4665–4678, 2019.

[7] A. Wedel *et al.*, “B-Spline Modeling of Road Surfaces With an Application to Free-Space Estimation,” *IEEE Transactions on Intelligent Transportation Systems*, vol. 10, no. 4, pp. 572–583, 2009.

[8] R. Fan *et al.*, “Pothole Detection Based on Disparity Transformation and Road Surface Modeling,” *IEEE Transactions on Image Processing*, vol. 29, pp. 897–908, 2019.

[9] R. Fan *et al.*, “Graph Attention Layer Evolves Semantic Segmentation for Road Pothole Detection: A Benchmark and Algorithms,” *IEEE Transactions on Image Processing*, vol. 30, pp. 8144–8154, 2021.

[10] C. Lu *et al.*, “Monocular Semantic Occupancy Grid Mapping With Convolutional Variational Encoder–Decoder Networks,” *IEEE Robotics and Automation Letters*, vol. 4, no. 2, pp. 445–452, 2019.

[11] C. Hazirbas *et al.*, “FuseNet: Incorporating Depth into Semantic Segmentation via Fusion-Based CNN Architecture,” in *13th Asian Conference on Computer Vision (ACCV)*. Springer, 2017, pp. 213–228.

[12] H. Wang *et al.*, “SNE-RoadSeg+: Rethinking Depth-Normal Translation and Deep Supervision for Freespace Detection,” in *2021 IEEE/RSJ International Conference on Intelligent Robots and Systems (IROS)*. IEEE, 2021, pp. 1140–1145.

[13] K. He *et al.*, “Deep Residual Learning for Image Recognition,” in *Proceedings of the IEEE Conference on Computer Vision and Pattern Recognition (CVPR)*, 2016, pp. 770–778.

[14] J. Fritsch *et al.*, “A New Performance Measure and Evaluation Benchmark for Road Detection Algorithms,” in *16th International IEEE Conference on Intelligent Transportation Systems (ITSC) 2013*. IEEE, 2013, pp. 1693–1700.

[15] K. Han *et al.*, “A Survey on Vision Transformer,” *IEEE Transactions on Pattern Analysis and Machine Intelligence*, vol. 45, no. 1, pp. 87–110, 2022.

[16] Z. Liu *et al.*, “Swin Transformer: Hierarchical Vision Transformer using Shifted Windows,” in *Proceedings of the IEEE/CVF International Conference on Computer Vision (ICCV)*, 2021, pp. 10012–10022.

[17] E. Xie *et al.*, “SegFormer: Simple and Efficient Design for Semantic Segmentation with Transformers,” *Advances in Neural Information Processing Systems (NeurIPS)*, vol. 34, pp. 12077–12090, 2021.

[18] K. Li *et al.*, “UniFormer: Unifying Convolution and Self-Attention for Visual Recognition,” *IEEE Transactions on Pattern Analysis and Machine Intelligence*, 2023.

[19] C. Min *et al.*, “ORFD: A Dataset and Benchmark for Off-Road Freespace Detection,” in *2022 International Conference on Robotics and Automation (ICRA)*. IEEE, 2022, pp. 2532–2538.

[20] P. Sun *et al.*, “Scalability in Perception for Autonomous Driving: Waymo Open Dataset,” in *Proceedings of the IEEE/CVF Conference on Computer Vision and Pattern Recognition (CVPR)*, 2020, pp. 2446–2454.

[21] M. Cordts *et al.*, “The Cityscapes Dataset for Semantic Urban Scene Understanding,” in *Proceedings of the IEEE/CVF Conference on Computer Vision and Pattern Recognition (CVPR)*, 2016, pp. 3213–3223.

[22] J. Long *et al.*, “Fully Convolutional Networks for Semantic Segmentation,” in *Proceedings of the IEEE/CVF Conference on Computer Vision and Pattern Recognition (CVPR)*, 2015, pp. 3431–3440.

[23] H. Ding *et al.*, “Context Contrasted Feature and Gated Multi-Scale Aggregation for Scene Segmentation,” in *Proceedings of the IEEE/CVF Conference on Computer Vision and Pattern Recognition (CVPR)*, 2018, pp. 2393–2402.

[24] L. Chen *et al.*, “Encoder–Decoder with Atrous Separable Convolution for Semantic Image Segmentation,” in *Proceedings of the European conference on computer vision (ECCV)*, 2018, pp. 801–818.

[25] J. Wang *et al.*, “Deep High-Resolution Representation Learning for Visual Recognition,” *IEEE Transactions on Pattern Analysis and Machine Intelligence*, vol. 43, no. 10, pp. 3349–3364, 2020.

[26] R. Strudel *et al.*, “Segmenter: Transformer for Semantic Segmentation,” in *Proceedings of the IEEE/CVF International Conference on Computer Vision (ICCV)*, 2021, pp. 7262–7272.

[27] S. Zheng *et al.*, “Rethinking Semantic Segmentation From a Sequence-to-Sequence Perspective With Transformers,” in *Proceedings of the IEEE/CVF Conference on Computer Vision and Pattern Recognition (CVPR)*, 2021, pp. 6881–6890.

[28] A. Dosovitskiy *et al.*, “An Image is Worth 16x16 Words: Transformers for Image Recognition at Scale,” *International Conference on Learning Representations (ICLR)*, 2020.

[29] B. Cheng *et al.*, “Per-Pixel Classification is Not All You Need for Semantic Segmentation,” *Advances in Neural Information Processing Systems (NeurIPS)*, vol. 34, pp. 17864–17875, 2021.

[30] Q. Ha *et al.*, “MFNet: Towards Real-Time Semantic Segmentation for Autonomous Vehicles with Multi-Spectral Scenes,” in *2017 IEEE/RSJ International Conference on Intelligent Robots and Systems (IROS)*. IEEE, 2017, pp. 5108–5115.

[31] Y. Sun *et al.*, “RTFNet: RGB–Thermal Fusion Network for Semantic Segmentation of Urban Scenes,” *IEEE Robotics and Automation Letters*, vol. 4, no. 3, pp. 2576–2583, 2019.

[32] Z. Liu *et al.*, “A ConvNet for the 2020s,” in *Proceedings of the IEEE/CVF Conference on Computer Vision and Pattern Recognition (CVPR)*, 2022, pp. 11976–111986.

[33] A. Radford *et al.*, “Learning Transferable Visual Models From Natural Language Supervision,” in *International Conference on Machine Learning (ICML)*. PMLR, 2021, pp. 8748–8763.

[34] T. Brown *et al.*, “Language Models are Few-Shot Learners,” *Advances in Neural Information Processing Systems (NeurIPS)*, vol. 33, pp. 1877–1901, 2020.

[35] P. Xu *et al.*, “Multimodal Learning with Transformers: A Survey,” *IEEE Transactions on Pattern Analysis and Machine Intelligence*, vol. 45, no. 10, pp. 12113–12132, 2023.

[36] J. Fu *et al.*, “Dual Attention Network for Scene Segmentation,” in *Proceedings of the IEEE/CVF Conference on Computer Vision and Pattern Recognition (CVPR)*, 2019, pp. 3146–3154.

[37] J. Hu *et al.*, “Squeeze-and-Excitation Networks,” in *Proceedings of the IEEE/CVF Conference on Computer Vision and Pattern Recognition (CVPR)*, 2018, pp. 7132–7141.

[38] S. Mai *et al.*, “Analyzing Multimodal Sentiment Via Acoustic- and Visual-LSTM With Channel-Aware Temporal Convolution Network,” *IEEE/ACM Transactions on Audio, Speech, and Language Processing*, vol. 29, pp. 1424–1437, 2021.

[39] F. Chollet, “Xception: Deep Learning With Depthwise Separable Convolutions,” in *Proceedings of the IEEE/CVF Conference on Computer Vision and Pattern Recognition (CVPR)*, 2017, pp. 1251–1258.

[40] B. Cheng *et al.*, “Masked-attention Mask Transformer for Universal Image Segmentation,” in *Proceedings of the IEEE/CVF Conference on Computer Vision and Pattern Recognition (CVPR)*, 2022, pp. 1290–1299.

[41] X. Zhu *et al.*, “Deformable DETR: Deformable Transformers for End-to-End Object Detection,” in *International Conference on Learning Representations (ICLR)*, 2020.

[42] J. Jain *et al.*, “OneFormer: One Transformer to Rule Universal Image Segmentation,” in *Proceedings of the IEEE/CVF Conference on Computer Vision and Pattern Recognition (CVPR)*, 2023, pp. 2989–2998.

[43] N. Carion *et al.*, “End-to-End Object Detection with Transformers,” in *European Conference on Computer Vision (ECCV)*. Springer, 2020, pp. 213–229.

[44] A. Dosovitskiy *et al.*, “CARLA: An Open Urban Driving Simulator,” in *Conference on Robot Learning (CoRL)*. PMLR, 2017, pp. 1–16.

[45] R. Fan *et al.*, “Road Surface 3D Reconstruction Based on Dense Subpixel Disparity Map Estimation,” *IEEE Transactions on Image Processing*, vol. 27, no. 6, pp. 3025–3035, 2018.

[46] R. Fan *et al.*, “Rethinking Road Surface 3-D Reconstruction and Pothole Detection: From Perspective Transformation to Disparity Map Segmentation,” *IEEE Transactions on Cybernetics*, vol. 52, no. 7, pp. 5799–5808, 2021.

[47] K. Perlin, “An Image Synthesizer,” *ACM Siggraph Computer Graphics*, vol. 19, no. 3, pp. 287–296, 1985.

[48] L. Lipson, Z. Teed, and J. Deng, “RAFT-Stereo: Multilevel Recurrent Field Transforms for Stereo Matching,” in *2021 International Conference on 3D Vision (3DV)*. IEEE, 2021, pp. 218–227.

[49] M. Menze and A. Geiger, “Object Scene Flow for Autonomous Vehicles,” in *Proceedings of the IEEE/CVF Conference on Computer Vision and Pattern Recognition (CVPR)*, 2015, pp. 3061–3070.

[50] Y. Feng, B. Xue, M. Liu, Q. Chen, and R. Fan, “D2nt: A high-performing depth-to-normal translator,” in *2023 IEEE International Conference on Robotics and Automation (ICRA)*, 2023, pp. 12 360–12 366.

[51] I. Loshchilov and F. Hutter, “Decoupled Weight Decay Regularization,” in *International Conference on Learning Representations (ICLR)*, 2018.

[52] L. Chen *et al.*, “DeepLab: Semantic Image Segmentation with Deep Convolutional Nets, Atrous Convolution, and Fully Connected CRFs,” *IEEE Transactions on Pattern Analysis and Machine Intelligence*, vol. 40, no. 4, pp. 834–848, 2017.

[53] H. Wang *et al.*, “Applying Surface Normal Information in Drivable Area and Road Anomaly Detection for Ground Mobile Robots,” in *2020 IEEE/RSJ International Conference on Intelligent Robots and Systems (IROS)*. IEEE, 2020, pp. 2706–2711.

[54] S. Gu *et al.*, “Histograms of the Normalized Inverse Depth and Line Scanning for Urban Road Detection,” *IEEE Transactions on Intelligent Transportation Systems*, vol. 20, no. 8, pp. 3070–3080, 2018.

[55] S. Gu *et al.*, “Road Detection through CRF based LiDAR-Camera Fusion,” in *2019 International Conference on Robotics and Automation (ICRA)*. IEEE, 2019, pp. 3832–3838.

[56] L. Sun *et al.*, “Pseudo-LiDAR-Based Road Detection,” *IEEE Transactions on Circuits and Systems for Video Technology*, vol. 32, no. 8, pp. 5386–5398, 2022.

[57] A. A. Khan *et al.*, “LRDNet: Lightweight LiDAR Aided Cascaded Feature Pools for Free Road Space Detection,” *IEEE Transactions on Multimedia*, 2022.